AGU PUBLICATIONS

Journal of Advances in Modeling Earth Systems



RESEARCH ARTICLE

10.1002/2016MS000865

# Imprint of the convective parameterization and sea-surface temperature on large-scale convective self-aggregation

**Tobias Becker**[1], **Bjorn Stevens**[1], **and Cathy Hohenegger**[1]

[1]Max Planck Institute for Meteorology, Hamburg, Germany

**Key Points:**
- The dependence of convective self-aggregation on SST is sensitive to the convective parameterization, in particular to the entrainment rate
- Self-aggregation dominates the statistics of the stationary state, partly masking the direct impact of the convective parameterization
- The SST dependence of convective self-aggregation is controlled by entrainment efficiency at high SSTs, and by a WISHE feedback at low SSTs

**Supporting Information:**
- Supporting Information S1
- Movie S1

**Correspondence to:**
T. Becker,
tobias.becker@mpimet.mpg.de

**Citation:**
Becker, T., B. Stevens, and C. Hohenegger (2017), Imprint of the convective parameterization and sea-surface temperature on large-scale convective self-aggregation, *J. Adv. Model. Earth Syst.*, *9*, doi:10.1002/2016MS000865.

Received 15 NOV 2016
Accepted 9 MAY 2017
Accepted article online 24 MAY 2017



**Abstract** Radiative-convective equilibrium simulations with the general circulation model ECHAM6 are used to explore to what extent the dependence of large-scale convective self-aggregation on sea-surface temperature (SST) is driven by the convective parameterization. Within the convective parameterization, we concentrate on the entrainment parameter and show that large-scale convective self-aggregation is independent of SST when the entrainment rate for deep convection is set to zero or when the convective parameterization is removed from the model. In the former case, convection always aggregates very weakly, whereas in the latter case, convection always aggregates very strongly. With a nontrivial representation of convective entrainment, large-scale convective self-aggregation depends nonmonotonically on SST. For SSTs below 295 K, convection is more aggregated the smaller the SST because large-scale moisture convergence is relatively small, constraining convective activity to regions with high wind-induced surface moisture fluxes. For SSTs above 295 K, convection is more aggregated the higher the SST because entrainment is most efficient in decreasing updraft buoyancy at high SSTs, amplifying the moisture-convection feedback. When halving the entrainment rate, convection is less efficient in reducing updraft buoyancy, and convection is less aggregated, in particular at high SSTs. Despite most early work on self-aggregation highlighted the role of nonconvective processes, we conclude that convective self-aggregation and the global climate state are sensitive to the convective parameterization.

## 1. Introduction

Parameterizing moist convection is one of the greatest challenges in climate system modeling [e.g., *Randall et al*., 2003; *Arakawa*, 2004; *Stevens and Bony*, 2013; *Bony et al*., 2015]. Moist convection is difficult to parameterize because it is strongly coupled to the environment through a diversity of processes, ranging from gravity waves to radiative transfer, moisture perturbations, and surface fluxes [e.g., *Bretherton and Smolarkiewicz*, 1989; *Bony and Emanuel*, 2005]. The coupling occurs on a variety of space and time scales, which makes it difficult to separate convective processes and convection-controlling processes. Here, we analyze radiative-convective equilibrium (RCE) simulations to understand how the convective parameterization, and in particular the entrainment parameter, controls the interaction of moist convection with the large-scale circulation, and how the governing mechanisms depend on the climate state.

With the RCE approach, the insolation and surface properties are assumed to be homogeneous and the planet is assumed to be nonrotating. The RCE approach has the advantages that it ensures a focus on the basic drivers of convection—radiation, tropospheric humidity, surface fluxes, and the convection-driven large-scale circulation—and that it is applicable in a hierarchy of models, bridging the gap between models that simulate convection and models that parameterize it. RCE has been used as a paradigm to understand climate for a long time [*Ramanathan and Coakley*, 1978, and references therein], but until recently the RCE framework has not been used in global models that parameterize convection. Running a general circulation model (GCM) in the RCE setup, as we do here, *Popke et al*. [2013] showed that RCE provides a good analog to the structure of the tropical circulation. Thus, RCE is emerging as an exciting new approach to address how parameterized convection interacts with its large-scale environment across all scales, and how the convective parameterization influences this coupling.

Convective organization may influence the interaction of convection and large-scale circulation. Observations show that organization emerges on all space scales in the climate system, with mesoscale organization contributing about 50% to tropical precipitation [*Nesbitt et al*., 2000]. Organization, and more specifically

convective aggregation, can be associated with a drying in the free troposphere and a decrease in low to midlevel cloud fraction in nonconvecting areas [*Tobin et al*., 2012]. The expansion of dry areas causes an increase in outgoing longwave radiation (OLR) and an increase in shortwave radiation absorbed by the surface. Convective aggregation thus modulates the strength and pattern of precipitation, and also influences the atmospheric moisture distribution, the radiation budget, and the large-scale circulation.

RCE studies with convection-permitting models show that convective self-aggregation is favored if domain size is larger than 200 km and if resolution is coarser than 2 km [*Muller and Held*, 2012; *Muller and Bony*, 2015]. Assuming that the mechanisms responsible for convective self-aggregation on the mesoscale in convection-permitting models also apply on the large scale in GCMs, this finding suggests that convection would always be extremely aggregated in GCMs. However, the few studies that use GCMs in the RCE configuration find a more diverse representation of RCE compared to their convection-permitting counterparts [*Coppin and Bony*, 2015; *Arnold and Randall*, 2015; *Bony et al*., 2016]. To some extent, the increase in diversity can be attributed to the convective parameterization, and to assumptions therein that have an impact on large-scale convective self-aggregation. The entrainment parameter has been shown to affect the coupling of convection to the large-scale flow in aquaplanet simulations [e.g., *Möbis and Stevens*, 2012; *Oueslati and Bellon*, 2013], and RCE simulations suggest that convective self-aggregation increases with the entrainment rate [*Arnold and Randall*, 2015].

Another research question is how convective self-aggregation depends on the prescribed SST. Here, the literature is less conclusive, with seemingly contradictory findings across studies. In two convection-permitting studies, convective self-aggregation is almost independent of SST [*Wing and Cronin*, 2016; *Holloway and Woolnough*, 2016], in other studies, both with convection-permitting models and GCMs, convective self-aggregation increases with SST [*Khairoutdinov and Emanuel*, 2010; *Wing and Emanuel*, 2014; *Arnold and Randall*, 2015; *Reed et al*., 2015], and with one GCM, convective self-aggregation even depends nonmonotonically on SST [*Coppin and Bony*, 2015]. The mechanisms that are responsible for the SST dependence include clear-sky longwave radiative feedbacks [*Emanuel et al*., 2014], radiation-circulation coupling [*Coppin and Bony*, 2015], and WISHE-circulation coupling [*Coppin and Bony*, 2015]. In this study, we combine both research questions, and analyze how the convective parameterization, and in particular the entrainment rate for deep convection, affects the dependence of large-scale convective self-aggregation on SST.

In section 2, we sketch the main features of the convective parameterization and outline our experimental strategy. Section 3 sets some terminology and gives a short overview over some results, whereas section 4 discusses how the RCE climate is mediated by assumptions in the convective parameterization—directly and through their effect on convective self-aggregation. In section 5, the response of the RCE climate to SST changes is discussed. The sensitivity of convective self-aggregation to SST and convection scheme arises as a particular point of emphasis. Section 6 briefly discusses the effect of self-aggregation on climate sensitivity. The study is summarized and concluded in section 7.

## 2. Methods

### 2.1. Convective Parameterization

In ECHAM6 [*Stevens et al*., 2013], the convective parameterization of *Nordeng* [1994] is used by default; hereafter "Nordeng" refers both to this parameterization and to model configurations that use it. To test ideas as to the cause of differences among models concerning the SST dependence of convective self-aggregation, three additional representations of convection are investigated. Two representations are based on Nordeng, with the only difference that the entrainment rate for deep convection is halved (HalfEntrN) or set to zero (NoEntrN), respectively, and one representation prohibits all subgrid-scale convection (NoCnvPm), in analogy to the Selected Process On/Off Klima Intercomparison Experiment [SPOOKIE, *Webb et al*., 2015]. The NoCnvPm setup can be envisioned as a configuration where the entrainment rate is set to infinite for every type of parameterized convection.

The Nordeng convection scheme uses the mass flux approach [*Arakawa and Schubert*, 1974; *Tiedtke*, 1989] and differentiates between shallow, midlevel and deep convection. Because midlevel convection is very rarely triggered, we do not discuss it further. The convection scheme is triggered if total moisture convergence below cloud base is positive, if updraft humidity is higher than in the environment and if the updraft is positively buoyant. For the triggering of deep convection, column-integrated total moisture convergence

must exceed surface evaporation by 10% and cloud depth has to be more than 200 hPa in the first updraft calculation. For deep convection, the closure for the cloud base mass flux is based on convective available potential energy (CAPE). CAPE is relaxed to zero with a prescribed time scale, which is 7200 s when using the spectral resolution T63 (corresponding to 1.875° resolution). The change of net upward mass flux $M_{up}$ with height depends on two qualitatively different types of mixing, turbulent (trb) and organized (org) mixing, expressed in the form of entrainment ($E$) and detrainment ($D$) of cumulus mass:

$$\frac{\partial M_{up}}{\partial z} = E_{trb} + E_{org} - D_{trb} - D_{org}. \quad (1)$$

By definition, turbulent entrainment is proportional to the mass flux itself, with different constants of proportionality for shallow and deep convection. Turbulent entrainment matches turbulent detrainment below the detrainment level $z_D$ and turbulent entrainment is set to zero above $z_D$. Organized entrainment and detrainment are enabled only in case of deep convection. Organized entrainment is parameterized as a function of updraft buoyancy, whereas organized detrainment is zero below the level of neutral buoyancy of a prescribed updraft, and is vertically distributed with a sine function above that level. In the simulations HalfEntrN and NoEntrN, where the entrainment rate for deep convection (hereafter entrainment rate) is changed by a certain factor, turbulent and organized entrainment as well as turbulent detrainment are multiplied by that factor. Organized detrainment is not changed to avoid that all of the detrainment is constrained to one level in NoEntrN.

For more details on the Nordeng convection scheme, the reader is referred to *Möbis and Stevens* [2012] because the implementation in ECHAM6 differs in some important details from what is described in the original publications.

### 2.2. Simulations

In all simulations, we use the general circulation model ECHAM 6.3 in a radiative-convective equilibrium configuration with T63 spectral resolution and 47 levels in the vertical. The main differences between this version of ECHAM6 and the version described by *Stevens et al*. [2013] are a correction to the faulty implementation of the cloud scheme that was identified in their paper, a better treatment of the thermodynamics in the cloud and convective parameterization to address energy conservation, and a different treatment of cloud-radiation interactions using the McICA approach and PSRad [*Pincus and Stevens*, 2013]. The RCE setup incorporates a spatially homogeneous diurnal cycle of insolation with a mean value of 340.3 W $m^{-2}$, no rotation of the planet and homogeneous conditions at the surface. The RCE setup is similar to the one described in more detail in *Popke et al*. [2013] and *Becker and Stevens* [2014], the only fundamental difference is that the RCE model is not coupled to a mixed layer ocean. Instead, we use globally uniform prescribed SSTs.

To understand how the SST dependence of large-scale convective self-aggregation is controlled by the convective parameterization, we have performed some sensitivity studies. We use four different representations of convection, Nordeng, HalfEntrN, NoEntrN, and NoCnvPm (defined in section 2.1), and we alter the SST at 5 K intervals in the range from 285 K to 305 K for all convective parameterization setups. Some additional simulations have been performed, including simulations where clouds are made invisible to radiation, similar to the Clouds On/Off Klima Intercomparison Experiments (COOKIE) [*Stevens et al*., 2012], but no surprise emerged. These simulations are only discussed in so far as they help understand one or the other aspect of the base simulations.

All simulations start from a homogeneous dry initial state and were run for 5 simulation years. In all simulations, equilibrium is reached after 1 year at the latest, so the last 4 years are analyzed. A check confirmed that results are statistically significant when looking at a 4-year average.

## 3. Quantifying Convective Self-Aggregation With Subsidence Fraction

Because convective aggregation has a strong impact on many different climate parameters, the degree of convective aggregation can be quantified in various ways. For example, convective aggregation can be quantified with the domain mean or spatial variance of outgoing longwave radiation, water vapor path, or surface fluxes [*Bretherton et al*., 2005; *Tobin et al*., 2012]. However, these quantities share the problem that

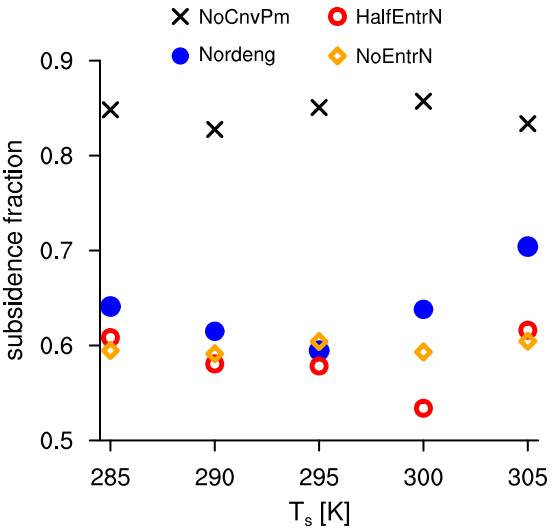


**Figure 1.** Area fraction where mass-weighted vertically integrated (1000 – 200 hPa) vertical velocity is directed downward, with different convective parameterizations and SSTs, averaged over all daily means in the analysis period. For all simulations, the range between the 25th and 75th percentile of daily-mean subsidence fraction is on the order of the respective symbol sizes. The standard error is estimated to be smaller than 0.002 (based on a 10 day autocorrelation time scale for the time-series of subsidence fraction).

they depend on SST, which would greatly complicate their application to our results. Parameters that do not depend on SST are, for example, column relative humidity or saturation fraction, defined as column water vapor path divided by saturation water vapor path [*Wing and Cronin*, 2016]. In this study, we quantify convective aggregation with subsidence fraction [*Coppin and Bony*, 2015; *Bony et al.*, 2016], another parameter that does not depend on SST. Subsidence fraction is estimated as the area where the mass-weighted vertically integrated (1000–200 hPa) and daily averaged vertical velocity is directed downward.

Figure 1 demonstrates that the variations of convective self-aggregation with SST strongly depend on the representation of convection. Convective self-aggregation is independent of SST in the two extreme convection scheme setups, with NoCnvPm and NoEntrN. With the two less extreme setups, Nordeng and HalfEntrN, we observe a nonmonotonic dependence of convective self-aggregation on SST. With Nordeng, self-aggregation decreases with SST for SSTs below 295 K, while above 295 K, self-aggregation increases with SST. With HalfEntrN, self-aggregation only increases with SST if SST is above 300 K. Mechanisms that can explain why convective self-aggregation depends on SST nonmonotonically and the reasons why the response differs with Nordeng and HalfEntrN are discussed in sections 5.2 and 5.3.

Independent of SST, convection is always most aggregated with NoCnvPm, Nordeng is in most of the simulations more aggregated than HalfEntrN and NoEntrN, and HalfEntrN is slightly more aggregated than NoEntrN at 285 K and 305 K, but less aggregated in between. Hence, with a few exceptions, higher entrainment rates can be associated with more convective self-aggregation, similar to what was found by *Arnold and Randall* [2015]. The following section analyzes why the degree of convective self-aggregation depends on the convective parameterization, and in particular on the entrainment parameter, restricting the analysis to the simulations with 305 K SST.

## 4. How Does the Convective Parameterization Affect Convective Self-Aggregation?

### 4.1. Horizontal Structure

Snapshots of precipitation and 10 m wind field, presented for the four different representations of convection in Figure 2, illustrate that in the global RCE model setup, convection aggregates on very large scales, with the largest convective systems being of the size of a continent. The snapshots also show that the simulations which aggregate more, like NoCnvPm but also Nordeng, have more clearly separated regions of subsidence and upward motion, larger individual subsidence regions, higher 10 m wind speeds, and more intense precipitation. In NoCnvPm, both the global mean 10 m wind speed and the difference between mean upward and mean downward velocity are almost three times larger than in NoEntrN (Table 1), confirming the impression of a much stronger overturning circulation in NoCnvPm than in NoEntrN. The increase of subsidence fraction is associated with a more pronounced increase of mean upward velocities in the convectively active areas than of mean downward velocities in the subsidence region (Table 1).

### 4.2. Vertical Structure

Because in our simulations convection aggregates in response to changes in the model physics, the results are not necessarily the same as in a transient run with constant model physics but varying aggregation. For a given degree of aggregation, we can expect that with a larger entrainment rate, more updrafts detrain in

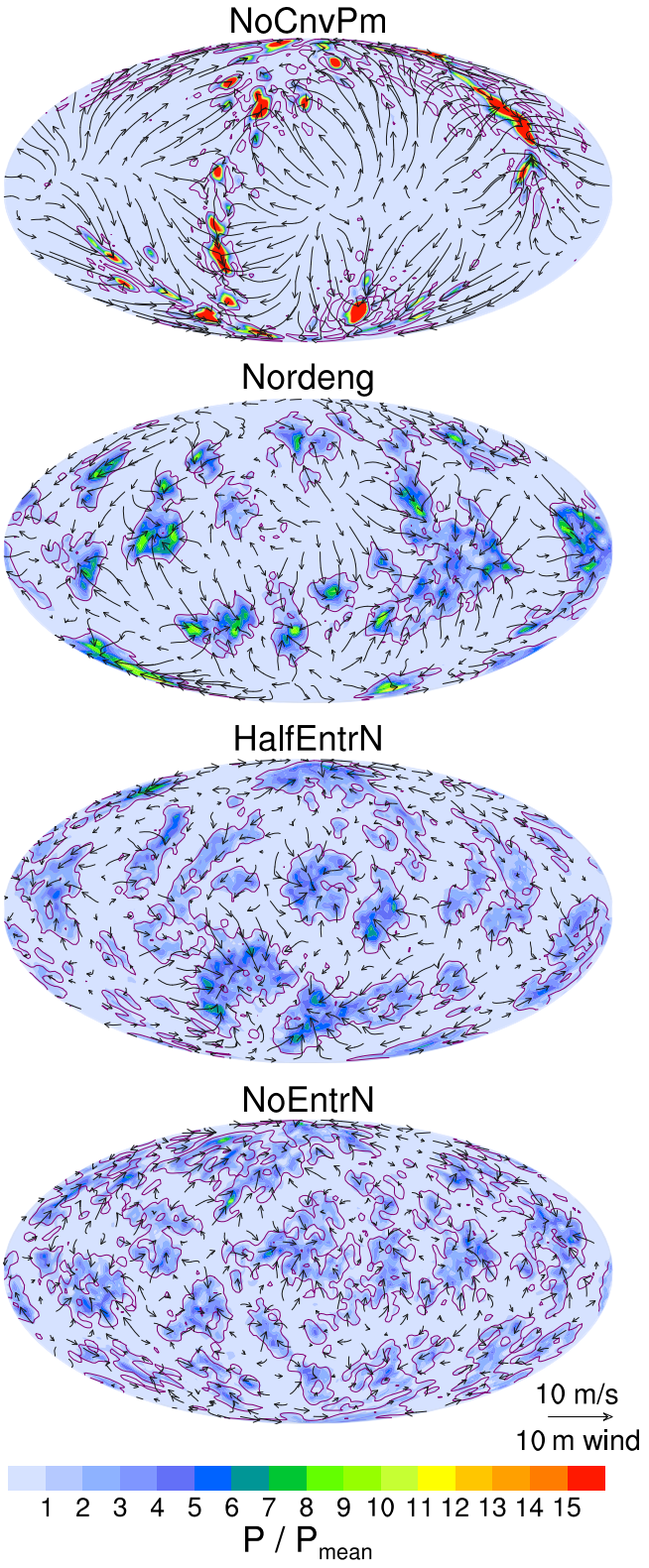


**Figure 2.** Random snapshots of precipitation relative to the global mean precipitation and 10 m wind field with different convective parameterizations at 305 K SST, averaged over 1 day. Purple contour lines distinguish subsidence and upward motion areas, indicating where daily averaged mass-weighted vertically integrated vertical velocities are zero.

the lower troposphere, moistening the lower troposphere and leading to more low clouds as compared to high clouds. For a given degree of aggregation, we can also expect the troposphere to be less stable with a larger entrainment rate because updrafts are more diluted, and therefore the concept of moist adiabatic ascent is less accurate. Those expectations are consistent with findings of *Tomassini et al.* [2015], who changed the entrainment rate in a coupled ocean-atmosphere model, in which convective aggregation plays less of a role. The question we answer in this subsection is whether those expectations are also fulfilled in the presence of convective aggregation.

Both in convection-permitting models [e.g., *Bretherton et al.*, 2005] and in observations [*Tobin et al.*, 2012], convective aggregation is accompanied by mid-tropospheric drying. However, in our simulations global mean free tropospheric relative humidity does not depend much on the degree of self-aggregation (Figure 3). Even though the subsidence region expands when aggregating and has a dry free troposphere (Figure 4), the larger subsidence region in more aggregated states does not project much on the mean state because the region with ascending air masses is moister in more aggregated states (Figure 4), almost balancing the drying on the global mean. The moistening of the region with ascending air masses does not only result from aggregation itself, including more vertical moisture advection by the resolved flow because of higher vertical velocities, but also results from changing the convective parameterization. Higher entrainment rates lead to an increase of relative humidity in the region with ascending air masses because high entrainment causes more organized detrainment at lower levels, which moistens the updraft's surrounding. In addition, updrafts with high entrainment rates concentrate in very moist columns wherein mixing does not strongly diminish updraft buoyancy.

**Table 1.** 10 m Wind Speed ($v_{10}$), Mean Upward Velocity ($\omega_{up}$), Mean Downward Velocity ($\omega_{down}$), and Subsidence Fraction (Area Fraction in Which the Daily Averaged Mass-Weighted Vertical Integral From 200 to 1000 hPa of Vertical Velocity is Directed Downward, SF) With Different Convective Parameterizations at 305 K SST, Averaged Over the Analysis Period

| Simulation | $v_{10}$ [m s$^{-1}$] | $\omega_{up}$ [hPa d$^{-1}$] | $\omega_{down}$ [hPa d$^{-1}$] | SF [%] |
|---|---|---|---|---|
| NoCnvPm | 5.5 | −124 | 25 | 83 |
| Nordeng | 3.0 | −53 | 22 | 70 |
| HalfEntrN | 2.2 | −36 | 22 | 62 |
| NoEntrN | 2.0 | −34 | 22 | 60 |

The moistening of the region with ascending air masses also leads to a higher precipitation efficiency and to less evaporating rain, decreasing water vapor residence time $t_v$, defined as the ratio of water vapor path to precipitation rate (Table 2). Had the circulation not changed, a higher entrainment rate would cause the opposite signal, an increase of $t_v$ due to more mixing. So, large-scale convective self-aggregation dominates the large-scale statistics, partly masking the direct but local effects from changing the entrainment rate that one might have expected had the circulation not changed.

Tropospheric stability increases with convective aggregation ($\Theta_{v_{200}} - \Theta_{v_{1000}}$ in Table 2) because convection occurs at a much warmer effective temperature, as explained in the next subsection. However, a consequence of changing the convective parameterization shows up in NoEntrN, where stability is high though convection is quite unaggregated. In the absence of entrainment, updrafts are fixed to the moist adiabat, stabilizing the temperature profile, in line with *Tomassini et al.* [2015]. Hence, small entrainment rates keep the updraft close to the moist adiabat, which increases stability, but small entrainment rates also cause convection to be less aggregated, which reduces stability. Overall, convective aggregation dominates, masking the direct effect from changing the entrainment rate that one might have expected had the circulation not changed.

In NoCnvPm, vertical moisture transport through convection is limited, leading to a high cloud fraction at the top of the boundary layer, whereas in NoEntrN, the lack of entrainment induces a large cloud fraction at the tropopause (Figure 3) because the updrafts do not mix with their environment and instead deposit all their moisture at the tropopause. Observations also show a tendency of more high clouds per unit low cloud in less aggregated environments [*Stein et al.*, 2017]. A study of *Bony et al.* [2016] also indicated that in less aggregated environments, anvil cloud fraction increases because stability close to the tropopause decreases, which implies that more clear-sky mass divergence is required to balance the vertical gradient in radiative cooling, leading to more extensive anvil clouds. This stability effect persists in our simulations, as the profiles of saturated moist static energy in Figure 3 illustrate. Thus, with respect to the vertical profile of cloud fraction, convective aggregation has the potential to amplify the direct effect from changing the entrainment rate.

Based on a more bottom-heavy profile of cloudiness in simulations with higher entrainment rates, we can expect a larger top-of-atmosphere (TOA) energy budget deficit. Convective aggregation perturbs the system in the same direction, also leading to a larger TOA energy budget deficit in more aggregated situations,

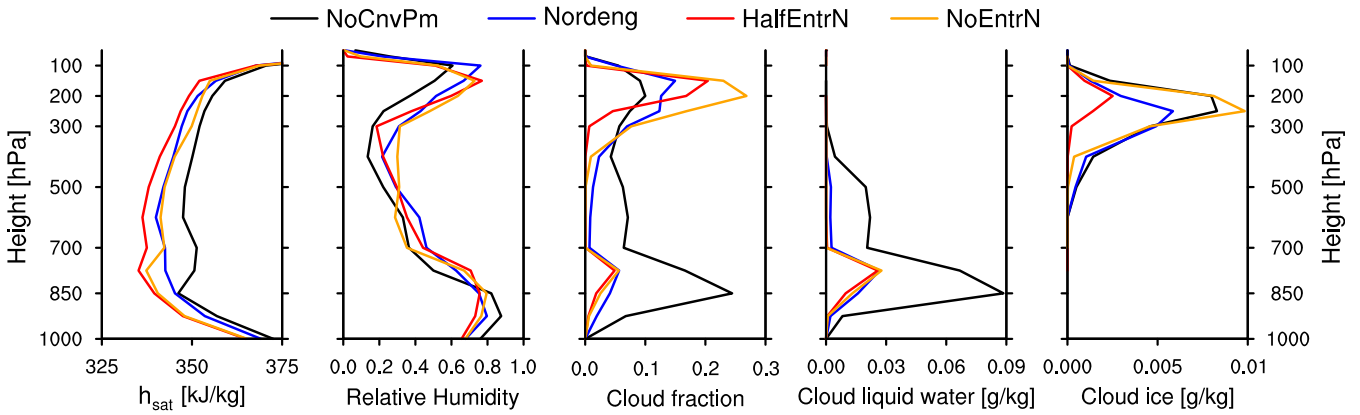


**Figure 3.** Profiles of atmospheric state variables with different convective parameterizations at 305 K SST, averaged over the analysis period and plotted as a function of pressure level. $h_{sat}$ is the saturated moist static energy.

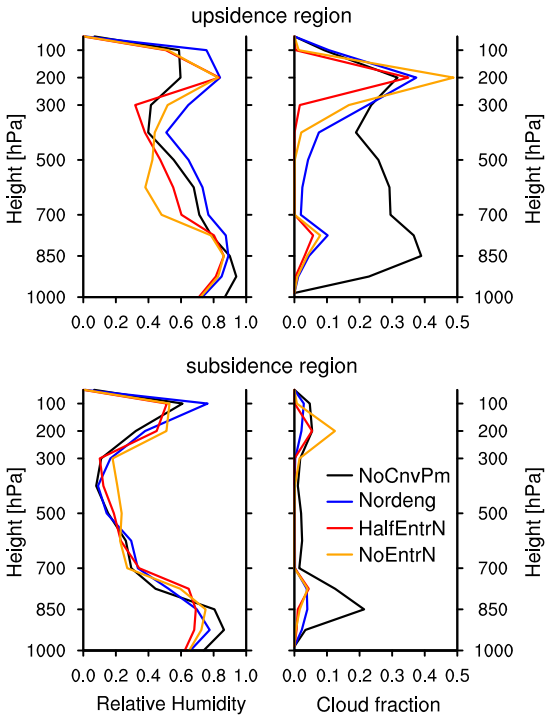


**Figure 4.** As Figure 3, but focusing on relative humidity and cloud fraction, and separating where daily averaged mass-weighted vertically integrated (1000 – 200 hPa) vertical velocity is directed downward (subsidence region) and upward (upsidence region).

both in observations [*Tobin et al.*, 2012] and models [*Hohenegger and Stevens*, 2016]. In our simulations, NoEntrN has indeed a 13 W $m^{-2}$ TOA energy budget surplus, while NoCnvPm has a 73 W $m^{-2}$ deficit (Table 2). In Nordeng, HalfEntrN, and NoEntrN, the changes of the TOA energy budget are primarily induced by changes in net atmospheric longwave cooling, which is in line with observations [*Tobin et al.*, 2012]. Larger subsidence regions associated with more convective self-aggregation cool more efficiently, inducing an increase of atmospheric longwave cooling, for example, by 23 W $m^{-2}$ in Nordeng compared to NoEntrN. Convective heating compensates, inducing rare but more intense precipitation which overcompensates on the global average the more frequent but less intense precipitation in less aggregated conditions (Table 2). Not in line with observations is that the negative TOA energy budget in NoCnvPm is caused by changes in absorbed solar radiation (ASR). In NoCnvPm, ASR is much smaller than with an activated convective parameterization because in the absence of parameterized shallow convection, a strong cloud-topped inversion at the top of the boundary layer develops (Figure 3). These low-level clouds have a strong impact on the radiation budget because they are prevalent in the subsidence region (Figure 4). In summary, the convective parameterization affects the vertical profile of moisture, temperature, and clouds, as well as the TOA energy budget directly. Nonetheless, the large-scale statistics are dominated by convective aggregation, either masking or amplifying the direct effects associated with the convective parameterization.

### 4.3. Moist Static Energy Distribution

To understand which processes govern the interaction of convection and large-scale circulation and are thus responsible for convective self-aggregation, we analyze the spatial distribution of moist static energy. Moist static energy is an invariant for moist adiabatic processes and is defined as

$$h = c_p T + gz + L_v q, \tag{2}$$

where $c_p$ is the isobaric specific heat capacity, $T$ is temperature, $g$ is gravity, $z$ is geopotential height, $L_v$ is the enthalpy of vaporization, and $q$ is specific humidity. The sum of the first two terms is also known as the dry static energy ($s$). Unlike other studies [*Wing and Emanuel*, 2014; *Arnold and Randall*, 2015], we neglect

**Table 2.** Precipitation ($P$), Water Vapor Residence Time (Ratio of Water Vapor Path to Precipitation Rate, $t_v$), Radiative Imbalance of the Atmosphere ($R_{atm}$), and at the Top-of-Atmosphere ($R_{TOA}$), Top-of-Atmosphere Outgoing Longwave Radiation (OLR), Top-of-Atmosphere Absorbed Solar Radiation (ASR) and Virtual Potential Temperature Difference Between 200 and 1000 hPa ($\Theta_{v_{200}} - \Theta_{v_{1000}}$) With Different Convective Parameterizations at 305 K SST, Averaged Over the Analysis Period

| Simulation | $P$ [mm $d^{-1}$] | $t_v$ [d] | $R_{atm}$ [W $m^{-2}$] | $R_{TOA}$ [W $m^{-2}$] | OLR [W $m^{-2}$] | ASR [W $m^{-2}$] | $\Theta_{v_{200}} - \Theta_{v_{1000}}$ [K] |
|---|---|---|---|---|---|---|---|
| NoCnvPm | 5.2 | 9.8 | −174 | −72.6 | 292 | 220 | 57.5 |
| Nordeng | 4.4 | 11.1 | −148 | −8.5 | 283 | 275 | 54.6 |
| HalfEntrN | 4.1 | 10.9 | −140 | 4.4 | 286 | 290 | 51.2 |
| NoEntrN | 3.7 | 12.7 | −126 | 13.4 | 267 | 281 | 55.0 |

the contribution of ice to moist static energy for reasons of simplicity and because the influence of frozen particles on the moist static energy budget is very small in the RCE setup. It also proves useful to analyze the mass-weighted vertical integral of $h$,

$$\langle h \rangle = \frac{1}{p_s - p_t} \int_{p_s}^{p_t} h \, dp, \tag{3}$$

with $p_s = 1000$ hPa and $p_t = 50$ hPa. The column longwave and shortwave net radiative fluxes in the atmosphere ($R_{atm,LW}$ and $R_{atm,SW}$), the latent and sensible heat release from the surface (LH and SH) and large-scale horizontal convergence of the flux of $\langle h \rangle$ ($\nabla_h \cdot \langle \vec{u} h \rangle$) are the only terms that can alter $\langle h \rangle$:

$$\frac{\partial \langle h \rangle}{\partial t} = R_{atm,LW} + R_{atm,SW} + LH + SH - \nabla_h \cdot \langle \vec{u} h \rangle \tag{4}$$

In the RCE setup, perturbations in temperature, or density, are damped and radiated away by gravity waves. These weak temperature gradient (WTG) conditions [*Sobel and Bretherton*, 2000] imply that horizontal anomalies in $h$ are essentially water vapor anomalies. For example, with Nordeng at 305 K, the standard deviation of $\langle h \rangle$, $\sigma_{\langle h \rangle}$, is 19 times larger than the standard deviation of $\langle s \rangle$, $\sigma_{\langle s \rangle}$. In all of the simulations, the distributions of $\langle h \rangle$ are very closely coupled to precipitation (Figure 5a). Upward motion (dashed line in Figure 5b) and precipitation only occur if $\langle h \rangle$ exceeds a certain value and precipitation intensifies depending on how much this value is exceeded.

The coupling of precipitation to $\langle h \rangle$ is weakest in NoEntrN, resulting in a more gradual increase of precipitation with increasing $\langle h \rangle$ (Figure 5a). For example, the correlation coefficient of $\langle h \rangle$ and precipitation is 0.68 with Nordeng, 0.69 with HalfEntrN and 0.63 with NoEntrN. With NoEntrN, the correlation coefficient is smaller than with Nordeng and HalfEntrN because the deactivation of entrainment decouples the convective updraft from its updraft environment, while in case of a high entrainment rate, precipitating convection can only occur in regions where the free troposphere is moist because otherwise entrainment of dry air would decrease updraft buoyancy too much [*Tompkins and Semie*, 2017]. Likewise, the detrainment also moistens the environmental air. The arguments hold only qualitatively for NoCnvPm (correlation coefficient of 0.43), as quantitatively the variability of precipitation across regions of high $\langle h \rangle$ weakens the relationship. Because of the simple budget equation and the close relation to precipitating convection, $\langle h \rangle$ is used in the following sections as an analysis tool to better understand convective self-aggregation.

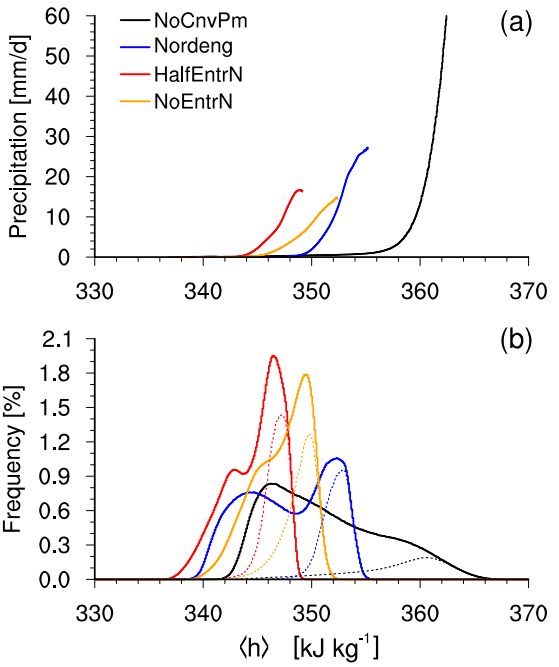


**Figure 5.** (a) Precipitation versus daily mean column-integrated $h$, at 0.05 kJ kg$^{-1}$ intervals, and (b) histograms of daily mean column-integrated $h$ (solid line: global; dashed: only in the region where column-integrated vertical velocity is directed upward), with a bin size of 0.1 kJ kg$^{-1}$. Presented are simulations with different convective parameterizations at 305 K SST.

With convective parameterizations that make it hard to trigger and maintain convection, mostly with NoCnvPm but also with Nordeng, $\langle h \rangle$ needs to be closer to $\langle h_{sat} \rangle$, so stronger $\langle h \rangle$ perturbations are necessary before precipitating convection occurs (Figure 5a). In case of scattered convection, detrainment cannot simply drive convectively active columns toward saturation because large-scale mixing is too strong. Hence, a strong overturning circulation associated with a high degree of convective self-aggregation is needed to efficiently transport enough water vapor into the convectively active regions and to increase updraft buoyancy by a sufficient amount to successfully produce precipitating convection. Thus, $\sigma_h$ increases in response to convective self-aggregation, also because the subsidence fraction increase leads to a shift of

weight toward low $h$ (Figure 5b). By stabilizing the subsidence region against convection, a large $\sigma_h$ favors self-aggregation. Convective self-aggregation is accompanied by a rise of the convecting temperature [*Held et al*., 1993; *Bretherton et al*., 2005], and the static stability of the troposphere increases in the whole domain, assuming WTG conditions. Thus, CAPE reduces and larger $h$ perturbations are necessary in the boundary layer for the onset of convection, in agreement with boundary-layer quasi-equilibrium theory [*Raymond*, 1997]. This makes it more unlikely that sufficient $h$ perturbations are created in the absence of a strong large-scale circulation. Cause and effect are hard to disentangle because large $h$ perturbations are only possible if convection is aggregated, and convective self-aggregation causes an increase in $\sigma_h$.

The increase of static stability with aggregation affects the distribution of $\langle h \rangle$, shifting the whole distribution toward higher values because of enhanced upper-tropospheric temperatures. The higher values of $\langle h \rangle$ in NoEntrN compared to HalfEntrN are not associated with self-aggregation, but with convection strictly following the moist adiabat because updrafts do not lose any buoyancy through entrainment. To conclude, the global reorganization of convection dominates the statistics of the RCE stationary state, partly masking the subtle differences in how convection couples to that state induced by the differences in the convective parameterization.

## 5. How Does the Convective Parameterization Affect the SST Dependence of Convective Self-Aggregation?

In this section, we analyze why convective self-aggregation depends non-monotonically on SST when using Nordeng, and why we find a different SST dependence with NoCnvPm, HalfEntrN, and NoEntrN. Both with Nordeng and HalfEntrN, the spatial pattern of self-aggregation depends on SST in a similar way (see supporting information Movie 1), suggesting that mechanisms that maintain self-aggregation are similar. The snapshots in Figure 6 illustrate that with Nordeng, convection aggregates at high SSTs in blobs, with diameters of about 5000 km, while it aggregates at low SSTs in arcs, with scales of up to 20,000 km in length. The arcs move rapidly toward the subsidence region with the strongest overturning circulation (Figure 6). At low SSTs, convective structures often travel to the other side of the planet within a week, while at high SSTs, they remain mostly at the same location in the same time frame (see supporting information movie). This emphasizes the need to use daily means or shorter time scales when analyzing subsidence fraction.

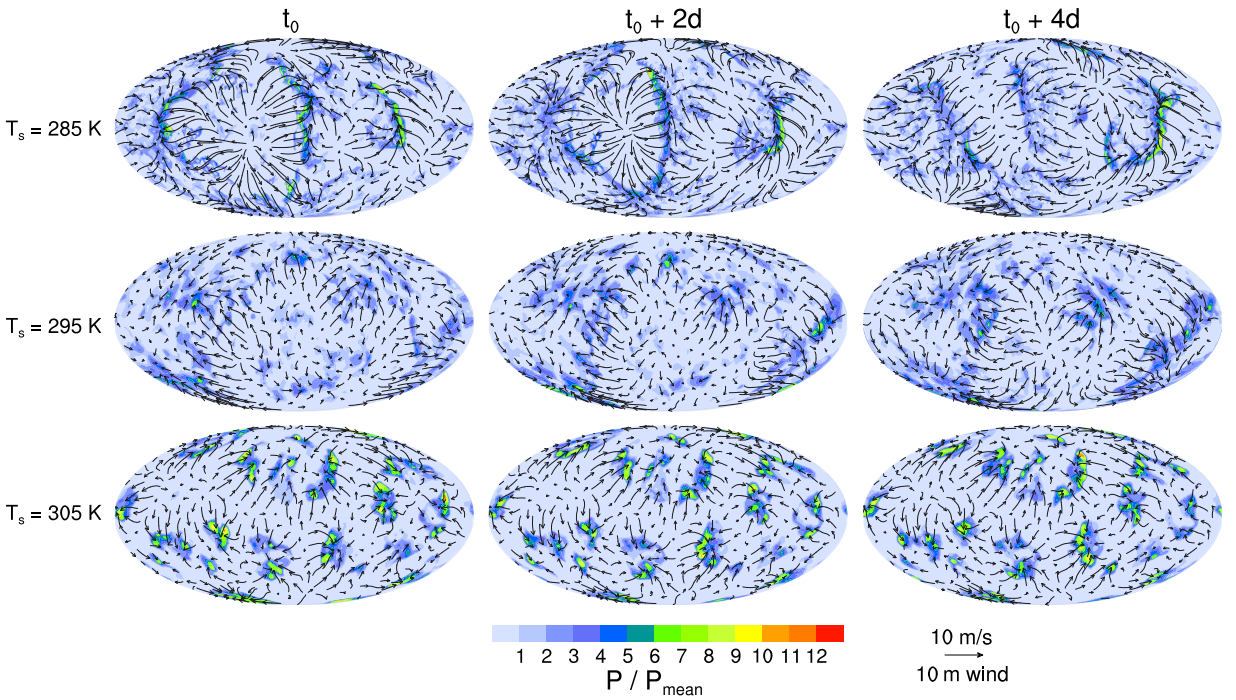


**Figure 6.** Random snapshots of precipitation relative to the global mean precipitation and 10 m wind field with Nordeng at three different SSTs, averaged over 1 day, showing also the consecutive snapshot 2 days later and 4 days later, respectively.

The enhanced cluster movement is also apparent in the global mean 10 m wind speed, which increases with decreasing SST, from 2.3 m $s^{-1}$ at 300 K to 3.8 m $s^{-1}$ at 285 K, also hinting at a stronger overturning circulation at lower SSTs. The slight recovery of surface winds at 305 K (2.9 m $s^{-1}$) associated with strong self-aggregation does not change the overall picture.

### 5.1. Moist Static Energy Variance Budget

As the analysis in section 4.3 has shown, high values of $\sigma_{\langle h \rangle}$ are associated with a high degree of convective self-aggregation. In this subsection, the spatial variance budget of $\langle h \rangle$ is analyzed with the goal to understand how the convective parameterization determines which physical processes are related to convective self-aggregation, and how these processes depend on SST. Following *Wing and Emanuel* [2014], we analyze factors influencing convective self-aggregation with the aid of the spatial moist static energy variance budget:

$$\frac{1}{2}\frac{\partial \langle h \rangle'^2}{\partial t} = \langle h \rangle' \mathrm{R}'_{\mathrm{atm,LW}} + \langle h \rangle' \mathrm{R}'_{\mathrm{atm,SW}} + \langle h \rangle' \mathrm{LH}' + \langle h \rangle' \mathrm{SH}' - \langle h \rangle' \nabla_{\mathrm{h}} \cdot \langle \vec{u} h \rangle. \quad (5)$$

Each term contains the covariance between $\langle h \rangle$ anomalies and $\langle h \rangle$ sources, or $\langle h \rangle$ convergence, respectively. Averaging over time and space and normalizing each term with $\overline{\langle h'^2 \rangle}$ yields the contribution of the different diabatic source terms to the growth rate of $\langle h \rangle$ variance, while normalizing with $\overline{\langle h \rangle}'$ yields the contribution to $\langle h \rangle$ standard deviation. To emphasize that, when identifying the governing mechanisms involved in self-aggregation, the absolute values are less important than the fractional contribution of each term relative to the other source terms, Figure 7 shows the contribution of each term to both $\overline{\langle h \rangle}'$ variance and to $\langle h \rangle$ standard deviation. Many studies have shown that the mechanisms that lead to self-aggregation and that sustain self-aggregation can differ substantially [e.g., *Muller and Held*, 2012]. Here, we focus on the mechanisms that sustain convective self-aggregation.

Convection-permitting studies show consistently that, given some initial self-aggregation, self-aggregation is maintained by cloud, water vapor, and radiation feedbacks because dry regions expand and confine convection into moister regions [*Bretherton et al.*, 2005; *Muller and Held*, 2012; *Jeevanjee and Romps*, 2013; *Wing and Emanuel*, 2014; *Muller and Bony*, 2015; *Bretherton and Khairoutdinov*, 2015; *Wing and Cronin*, 2016; *Holloway and Woolnough*, 2016; literature overview by *Mapes*, 2016]. In accordance with this, Figure 7 shows that in all of the simulations, except with HalfEntrN below 295 K, the longwave net atmospheric flux is the dominant source of $\langle h \rangle$ variance, maintaining convective self-aggregation in the equilibrium state. The reason is that in convectively active regions, clouds and enhanced water vapor concentrations increase the effective longwave emission height, thus reducing the atmosphere's longwave cooling in regions of high $\langle h \rangle$, while

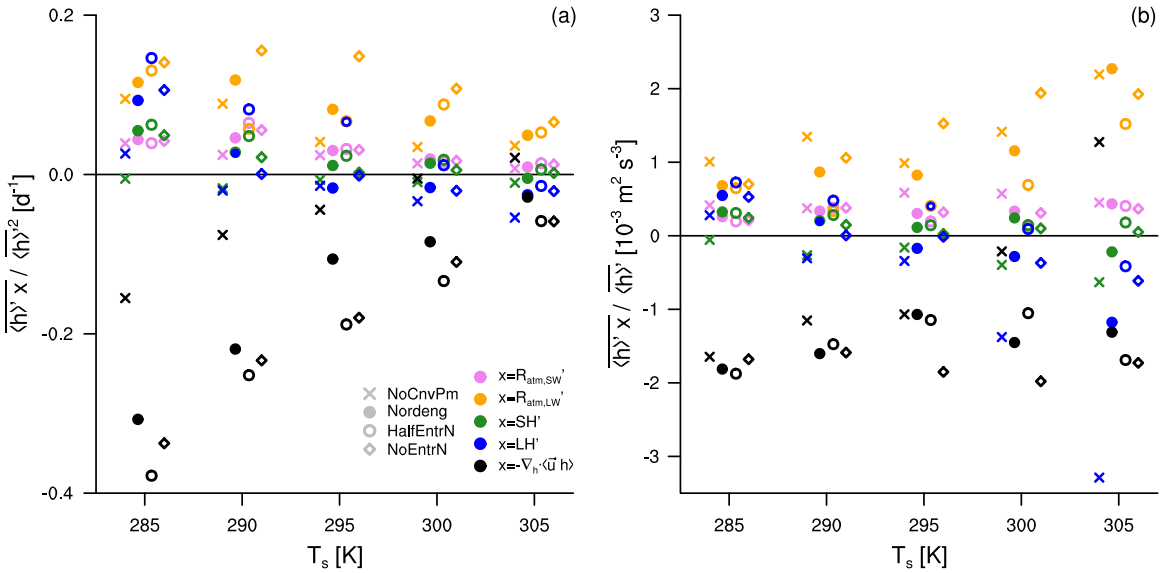


**Figure 7.** Covariance of column-integrated moist static energy $\langle h \rangle$ and different sources of $\langle h \rangle$, averaged over the analysis period and (a) scaled with the global average of $\langle h \rangle$ variance, or (b) scaled with the global average of $\langle h \rangle$ standard deviation. The large-scale horizontal convergence of the flux of $\langle h \rangle$ is the residual.

dry subsidence regions have low effective emission heights, thus accelerating the atmosphere's cooling in regions of low $\langle h \rangle$. In NoEntrN, more condensate is detrained at higher levels. This leads to even more high clouds in the convectively active region, amplifying the cloud-radiative effect.

The net shortwave irradiance is an additional source of $\langle h \rangle$ variance in all simulations because clear-sky atmospheric shortwave absorption increases with column water vapor, but the magnitude of this effect is much smaller than the longwave radiative feedback. Surface fluxes and especially latent heat release are sources of $\langle h \rangle$ variance at low SSTs. This turns out to be very important for convective self-aggregation at low SSTs, as discussed in more detail in section 5.2. The large-scale horizontal convergence of the flux of $\langle h \rangle$, which is calculated as residual from the budget, is a sink of $\langle h \rangle$ variance in almost all of the simulations, which means that the circulation is thermally direct, as it transfers moist static energy from high-$h$ regions to low-$h$ regions. However, the fractional contribution of $\langle h \rangle$ convergence to the $\langle h \rangle$ variance budget decreases with increasing SST (Figure 7).

### 5.2. Which Mechanisms Reinforce Convective Self-Aggregation at Low SSTs?

An increase of convective self-aggregation with decreasing SST has so far only been found by *Coppin and Bony* [2015] with the IPSL model in RCE mode. They explain the increase of convective self-aggregation at SSTs below 300 K with a more effective cooling from low clouds in the subsidence region, leading both to the formation of radiatively driven cold pools, and to a low-level overturning circulation. In ECHAM6-RCE, convective self-aggregation increases with decreasing SST at SSTs below 295 K with Nordeng, and below 300 K with HalfEntrN (Figure 1), while NoEntrN and NoCnvPm do not show any SST dependence.

Surface fluxes have the potential to be very important for convective self-aggregation because anomalies in sensible or latent heat flux are sources of $h$ perturbations in the boundary layer. Properties which can influence surface fluxes are SST, wind speed, relative humidity, and stability at the lowest model level. At low SSTs, the latent heat flux tends to be stronger in regions of large $\langle h \rangle$ and is a source of $\langle h \rangle$ variance (Figure 7). This is counter-intuitive because, all else being equal, high $h$ perturbations in the boundary layer imply less latent heat flux because $h$ perturbations mostly reflect humidity perturbations. However, the lower the SST, the less do perturbations in latent and sensible heat flux depend on relative humidity and stability anomalies, but are dominated by the wind speed (Figure 8). The wind speed itself also shows an SST dependence. With Nordeng, at high SSTs, wind speeds maximize close to the median of $\langle h \rangle$ and differ only by about 1 m $s^{-1}$, while at low SSTs, wind speeds in high $\langle h \rangle$ regions are on average more than 3 m $s^{-1}$ higher than winds in low $\langle h \rangle$ regions (Figure 8a). Thus, sensible and especially latent heat fluxes are important for convective self-aggregation at low SSTs due to a stronger coupling of surface fluxes to the wind speed and due to a changing wind pattern.

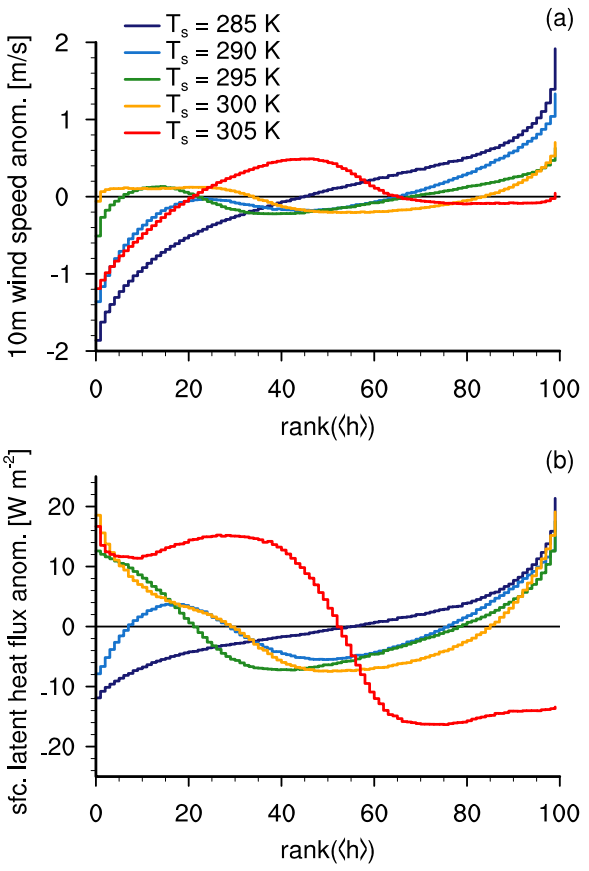


**Figure 8.** (a) Anomaly of 10 m wind speed and (b) surface latent heat flux, sorted by column-integrated moist static energy, for five different SSTs with Nordeng, using daily mean values averaged over the analysis period.

The local moisture supply through surface evaporation, which becomes more important at low SSTs, can explain the changing wind pattern. As Figure 6 (see also supporting information movie) demonstrates, at low

**Table 3.** Ratio of the Daily-Averaged Absolute Value of Vertically Integrated Moisture Convergence and of Surface Moisture Flux ($|\nabla_h \cdot \langle \vec{u}q \rangle| / (E\,g/p_s)$), Column Water Vapor ($\langle q \rangle$), Precipitation ($P$), Water Vapor Residence Time ($t_v$), Vertical Velocity in the Subsidence Region ($\omega_{sub}$), and Virtual Potential Temperature Difference Between 300 and 1000 hPa ($\Theta_{v_{300}} - \Theta_{v_{1000}}$) With Different SSTs in Nordeng, Averaged Over the Analysis Period

| Simulation | $\lvert\nabla_h \cdot \langle \vec{u}q \rangle\rvert / (E\,g/p_s)$ | $\langle q \rangle$ [kg m$^{-2}$] | $P$ [mm d$^{-1}$] | $t_v$ [d] | $\omega_{sub}$ [hPa d$^{-1}$] | $\Theta_{v_{300}} - \Theta_{v_{1000}}$ [K] |
|---|---|---|---|---|---|---|
| 285 K | 1.20 | 8.6 | 2.3 | 3.8 | 36.8 | 15.0 |
| 290 K | 1.26 | 14.0 | 2.8 | 5.1 | 30.7 | 19.4 |
| 295 K | 1.56 | 21.7 | 3.1 | 7.0 | 25.8 | 24.9 |
| 300 K | 2.38 | 31.1 | 3.4 | 9.1 | 23.8 | 30.6 |
| 305 K | 3.17 | 49.0 | 4.4 | 11.1 | 22.2 | 46.2 |

SSTs convection favors the edges of the largest subsidence regions. At the edges, the low-level flow converges, creating more favorable conditions for convective activity, in particular because the high surface wind speeds induce high surface heat fluxes (WISHE feedback). The size of large subsidence regions decreases with time because convective structures propagate toward the center of the subsidence region, always seeking the strongest surface fluxes, until the edges of another subsidence region are more favorable for convection. This is the reason for the fast movement of the convective structures at low SSTs. Because of these dynamics, it is not surprising that the ratio of the globally averaged absolute value of vertically integrated moisture convergence, $|\nabla_h \cdot \langle \vec{u}q \rangle|$, and of surface moisture flux, $E$, shows an SST dependence. The resulting dimensionless number $\gamma$, which describes how much water vapor in a column stems from horizontal convergence relative to surface evaporation, is close to 1 at low SSTs, and overall shows an increase of about 4.7% K$^{-1}$, although less pronounced at low SSTs (Table 3).

Using thermodynamic reasoning, we can understand why, at low SSTs, surface moisture fluxes are relatively more important than horizontal moisture convergence for the onset of convection. In equilibrium state, $E$ is equal to precipitation $P$, and $|\nabla_h \cdot \langle \vec{u}q \rangle|$ can be assumed to scale with the product of column water vapor $\langle q \rangle$ and the average vertical velocity in the subsidence region, $\omega_{sub}$, from which the strength of the large-scale overturning circulation can be inferred. The ratio of $\langle q \rangle$ and $P$ defines the water vapor residence time $t_v$. So in total, $\gamma$ can be constrained by

$$\gamma \sim \frac{|\nabla_h \cdot \langle \vec{u}q \rangle|}{E} \sim \frac{\langle q \rangle}{P}\,\omega_{sub} \sim t_v\,\omega_{sub}. \tag{6}$$

For a given strength of circulation, $t_v$ measures how local the precipitation is: a shorter residence time implies that precipitation forms near where it evaporates, and suggests that latent heat fluxes are more important for precipitation than they would be for the same circulation but a longer residence time. With decreasing SST, $t_v$ strongly decreases because $\langle q \rangle$ changes more with SST than $P$ does. In Nordeng, $\langle q \rangle$ increases with 9.1% K$^{-1}$ (Table 3), and thus is in the same range as in other studies [*O'Gorman and Muller*, 2010; *Muller et al*., 2011]. While there is a super Clausius-Clapeyron (CC) scaling of $\langle q \rangle$, precipitation depends less on temperature than CC [*Held and Soden*, 2006]. In Nordeng, precipitation increases with 3.2% K$^{-1}$ (Table 3), which is, compared to the hydrological sensitivity parameter in other studies [*Fläschner et al*., 2016], a rather large rate of increase. The differences in SST dependence of $\langle q \rangle$ and $P$ result in an increase of $t_v$ by 5.7% K$^{-1}$ (Table 3). Hence, in the absence of a changing large-scale circulation, precipitating convection is more tied to local surface moisture fluxes at low SSTs.

The average vertical velocity in the subsidence region, $\omega_{sub}$, decreases in Nordeng by about $-3.5\%$ K$^{-1}$ at low SSTs and by about $-1.5\%$ K$^{-1}$ at high SSTs (Table 3). The subsidence velocity is thermodynamically constrained by the ratio of diabatic cooling $Q$ and static stability. The diabatic cooling, which is primarily longwave cooling, does not increase at low SSTs, if anything, it decreases (Figure 9). Thus, the increase in subsidence velocity (Figure 9) must be caused by a strong decrease in static stability, which overcompensates the decrease in $Q$. Considering the whole troposphere, in radiative-convective equilibrium $Q$ is proportional to $P$ and stability can be approximated from the virtual potential temperature difference between 1000 and 300 hPa:

$$\omega_{sub} \sim \frac{Q}{\partial\Theta_v/\partial p} \sim \frac{P}{\Theta_{v_{300}} - \Theta_{v_{1000}}}. \tag{7}$$

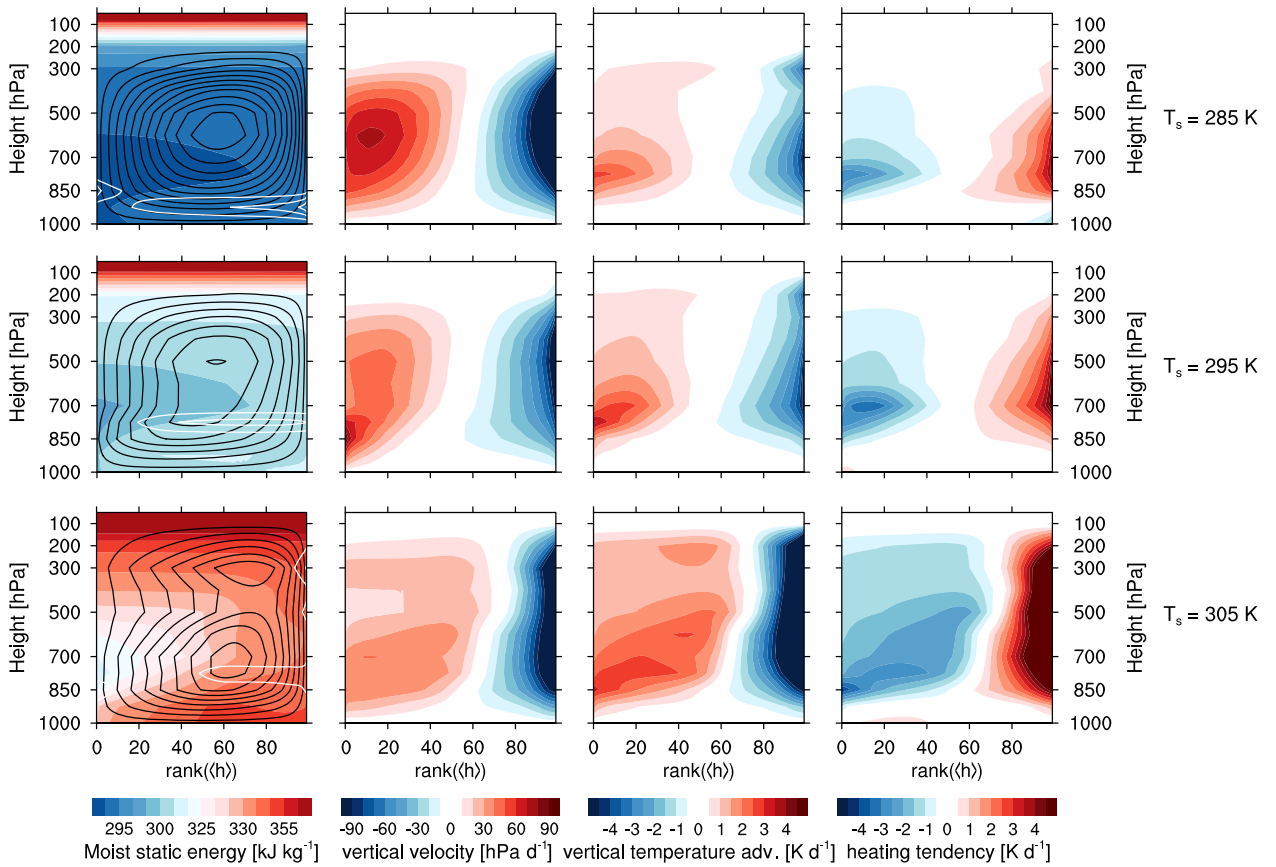


**Figure 9.** Moist static energy, contours of stream function (in black, counterclockwise, every 0.02 kg $m^{-2}$ $s^{-1}$) and contours of cloud water content (liquid + ice, in white, every 0.03 g $kg^{-1}$) (first column), vertical velocity (second column), warming associated with vertical motion (third column), and diabatic heating tendency (fourth column), plotted as a function of pressure level and column-integrated moist static energy, for three different SSTs with Nordeng, using daily mean values averaged over the analysis period.

When constraining subsidence velocity with this approximation, a decrease rate of $-2.2\%$ $K^{-1}$ results (Table 3). In total, based on equations (6) and (7), $\gamma$ is thermodynamically constrained to increase with 3.4% $K^{-1}$, which is a bit less than the actual rate of increase, 4.7% $K^{-1}$. The difference between the thermodynamically constrained and actual rate of increase of $\gamma$—as well as the SST-dependence of the actual rate of increase of $\gamma$—can mostly be explained with changes in convective self-aggregation. A higher degree of self-aggregation is accompanied by a stronger overturning circulation and higher subsidence velocity. This explains why $\gamma$ increases relatively slowly with SST as long as convective aggregation decreases with SST (below 295 K), while $\gamma$ increases much faster as soon as convective aggregation increases with SST.

Below 295 K, convective self-aggregation increases with a similar rate with decreasing SST both with Nordeng and HalfEntrN due to the WISHE feedback. In NoEntrN, the WISHE feedback is less effective because convection is less inhibited in the subsidence region, which is necessary for the formation of large subsidence regions. In NoCnvPm, convection is too slow to react to the wind-induced variations in surface fluxes. Irrespective of that, NoCnvPm is extremely aggregated because of the extremely high $h$ perturbations that are required in the boundary layer for the onset of large-scale convection (see section 4.3). The WISHE feedback is independent of cloud-induced cooling because when disabling the cloud-radiative effects in Nordeng, at low SSTs surface fluxes are similarly large sources of $\langle h \rangle$ variance as with enabled cloud-radiative effects. This outcome differs from *Coppin and Bony* [2015], as in their model enhanced longwave cooling from low-level clouds is crucial for cold pool expansion and the initialization of convective self-aggregation at low SSTs.

### 5.3. Which Mechanisms Reinforce Convective Self-Aggregation at High SSTs?

An increase of convective self-aggregation with SST has been found with some GCMs [*Coppin and Bony*, 2015; *Arnold and Randall*, 2015] and some convection-permitting models [*Khairoutdinov and Emanuel*, 2010; *Wing and Emanuel*, 2014; *Hohenegger and Stevens*, 2016], but with other convection-permitting models,

only a very weak SST dependence was found [*Wing and Cronin*, 2016; *Holloway and Woolnough*, 2016], and the governing mechanisms appear to differ among the models. On the one hand, *Emanuel et al.* [2014] explain the SST dependence of convective self-aggregation with a temperature-dependent moisture-longwave radiation feedback, on the other hand, *Beucler and Cronin* [2016] show that the longwave feedback likely is temperature-dependent, but that clouds and the vertical structure of humidity perturbations can strongly modulate this, and, as a consequence, the longwave feedback could favor self-aggregation even at lower SSTs. In contrast, *Coppin and Bony* [2015] relate the increase of convective self-aggregation at high SSTs to a strengthening of the WISHE feedback.

In our model, the WISHE feedback cannot sustain convective self-aggregation at high SSTs because the covariance of $\langle h \rangle$ and surface fluxes is negative at high SSTs, decreasing the $\langle h \rangle$ variance (Figure 7). Instead, the fractional contribution of the moisture-radiation feedback to $\langle h \rangle$ variance increases with SST (Figure 7). However, another self-aggregation mechanism is more directly related to the convective parameterization and is of most importance at high SSTs. The vertical profiles in Figure 10 show that the SST increase induces a temperature increase throughout the whole troposphere, while the relative humidity profile depends nonsystematically on SST, changing only by about 10% in the low troposphere. Consequently, the absolute humidity difference between the saturated air in the updraft and the environmental air increases, which means that the same amount of entrained air can cause more evaporative cooling in the updraft. Hence, the higher the SST, the more effective is entrainment in reducing updraft buoyancy. This is in agreement with *Singh and O'Gorman* [2013] who find that an increase of saturation deficit with SST is accompanied by an increase of CAPE. Greater saturation deficits require higher $h$ perturbations and, as section 4.3 has shown, large $h$ perturbations are associated with a high degree of convective self-aggregation (and vice versa).

The SST-dependent entrainment efficiency explains why a moisture-convection feedback [or water vapor-convection feedback, *Tompkins and Semie*, 2017] strengthens with increasing SST. Although *Emanuel et al.* [2014] argue that a moisture-convection feedback is not crucial for self-aggregation, *Craig and Mack* [2013] claim that it is the fundamental feedback. As this moisture-convection feedback directly depends on the convective parameterization, convective self-aggregation is more parameterization-dependent at high SSTs than at low SSTs. Convective self-aggregation increases at high SSTs most with Nordeng, where convection is most sensitive to entrainment, while the increase of convective self-aggregation is weaker and only starts at a higher SST when the entrainment rate is halved (HalfEntrN). In the two extreme cases, NoEntrN and NoCnvPm, convective self-aggregation does not increase at high SSTs because in the first case, no environmental unsaturated air is entrained into the updraft and in the second case, the explicit, large-scale convection is only weakly influenced by large-scale mixing.

Another mechanism which is commonly associated with convective self-aggregation, an upgradient transport of $h$ by a low-level overturning circulation [*Bretherton et al.*, 2005; *Muller and Held*, 2012; *Wing and Emanuel*, 2014; *Muller and Bony*, 2015], is apparent at high SSTs with Nordeng (Figure 9). A low-level overturning

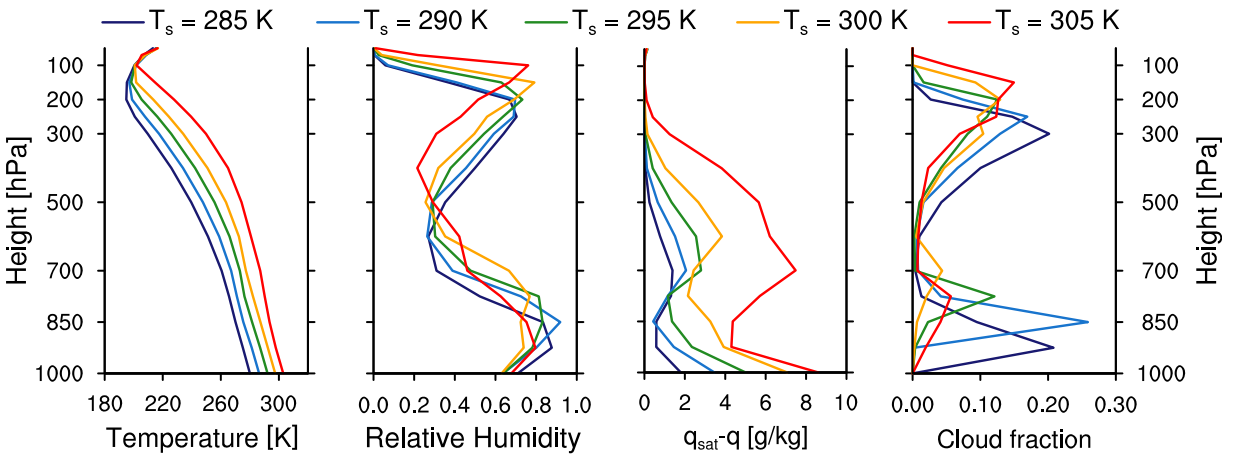


**Figure 10.** Profiles of atmospheric state variables for different SSTs with Nordeng, averaged over the analysis period and plotted as a function of pressure level. $q_{sat} - q$ is the difference between saturated specific humidity and domain-mean specific humidity.

**Table 4.** Top-of-Atmosphere Radiation Imbalance $R_{TOA}$, in W m$^{-2}$ [a]

| Simulation | 285 K | 290 K | 295 K | 300 K | 305 K |
|---|---|---|---|---|---|
| NoCnvPm | −14.0 | −32.7 | −38.1 | −58.2 | −72.6 |
| Nordeng | 22.8 | 7.4 | 6.8 | 15.7 | −8.5 |
| HalfEntrN | 26.7 | 11.0 | 16.4 | 23.8 | 4.4 |
| NoEntrN | 32.6 | 20.7 | 29.9 | 26.0 | 13.3 |

[a]A strong decrease of $R_{TOA}$ with SST implies a small climate sensitivity.

circulation causes an upgradient $h$ transport, partly compensating the downgradient $h$ transport by the deep overturning circulation. The overall $h$ transport, calculated from the stream function in Figure 9, is 29%, smaller at 305 K than at 300 K SST. For the formation of the low-level overturning circulation, a cooling profile in the subsidence region that is more bottom-heavy than the stability profile is the key ingredient (following equation (7)). However, though radiative cooling from low clouds has been found to be a necessary condition for a low-level overturning circulation during the initialization of self-aggregation [*Muller and Held*, 2012], this is not a necessary condition in the later stages of self-aggregation discussed here because the low-level circulation prevails even when cloud-radiative effects are disabled. Instead, a strong gradient in relative humidity at the top of the boundary layer is sufficient to cause enough low-level cooling to trigger the low-level overturning circulation. The low-level overturning circulation occurs at high SSTs with Nordeng, HalfEntrN, and NoEntrN, and the governing mechanisms seem to be relatively independent of the convective parameterization.

## 6. Does Convective Self-Aggregation Have an Effect on Climate Sensitivity?

Climate sensitivity can be estimated from simulations with different prescribed SSTs based on how the TOA energy budget changes with SST, in analogy to *Cess et al*. [1989, 1990, 1996] and many others. Over the whole range of SSTs, the TOA energy budget changes most with NoCnvPm, followed in decreasing order by Nordeng, HalfEntrN, and NoEntrN (Table 4). Thus, simulations with strong self-aggregation have on average smaller climate sensitivities. This is presumably related to the uneven horizontal distribution of cloud and water vapor, reducing the impact of two positive feedbacks, the cloud and water vapor feedback. In those simulations where self-aggregation increases with SST, with Nordeng and HalfEntrN at high SSTs, climate sensitivity is small (Table 4). However, these results should be interpreted with caution because climate sensitivity varies very strongly among the simulations, and there are some ranges where the TOA energy imbalance increases with SST, suggesting that in a mixed-layer ocean simulation there could be jumps between a warm state and a cold state within some simulations. These occurrences of implied negative climate sensitivity are associated with low-level cloud fraction changes (Figure 10), leading to strong rates of increase of absorbed solar radiation with SST.

## 7. Summary and Conclusions

In this study, we examine how the SST dependence of large-scale convective self-aggregation depends on the convective parameterization. For this purpose, we use the general circulation model ECHAM6 in a non-rotating RCE framework and perform a sensitivity study, changing both the globally uniform SST and the convective parameterization, in particular the entrainment rate. In the analysis, we focus on the stationary state to infer from the large-scale statistics, for example, from the vertically integrated distribution of moist static energy ($h$), how convection couples to the large-scale circulation, and how the mechanisms that sustain convective self-aggregation differ among the simulations.

We find that the convective parameterization alters the structure of the troposphere through a global reorganization of the large-scale circulation. The emergence of self-aggregation dominates the large-scale statistics, making it difficult to find the trace of how convection is parameterized in the statistics, beyond the fact that the degree of convective self-aggregation depends substantially on the way in which convection is parameterized. The higher the entrainment rate, the higher the buoyancy at cloud base has to be to compensate for the less buoyant air that gets entrained. Stronger perturbations of moist static energy in the boundary layer are associated with enhanced convective self-aggregation for two reasons. First, strong $h$ perturbations can only be created if convection is aggregated on large scales. And second, the high

variance of $h$ stabilizes the subsidence region against convection. Whether the $h$ perturbations cause self-aggregation, or whether self-aggregation creates the $h$ perturbations, cannot be distinguished, they just come together.

Large-scale convective self-aggregation is independent of SST when setting the entrainment rate for deep convection to zero, or when removing the convective parameterization from the model. In the first case self-aggregation is always weak, while in the latter case self-aggregation is always very strong. With a non-trivial representation of convective entrainment, we observe a nonmonotonic dependence of large-scale convective self-aggregation on SST. At low SSTs, the large-scale water vapor transport is relatively small compared to local surface fluxes, constraining convective activity to regions with high wind-induced surface moisture fluxes. Thus, for SSTs below 295 K, the increase of convective self-aggregation with decreasing SST can be explained with the wind-induced surface heat exchange (WISHE) feedback being most important at low SSTs. With Nordeng, convective self-aggregation increases with SST for SSTs above 295 K, while when halving the entrainment rate (HalfEntrN), self-aggregation only increases with SST for SSTs above 300 K. The reason is that the saturation deficit increases with increasing SST, enabling the same amount of entrained air to reduce updraft buoyancy much more efficiently, strengthening the moisture-convection feedback. Consequently, the setup with the highest entrainment rate (Nordeng) shows the strongest increase of convective self-aggregation at high SSTs because larger $h$ perturbations and more convective self-aggregation are necessary to sustain deep convection in a warm atmosphere. Additionally, a strong moisture-longwave radiation feedback and a low-level overturning circulation help to maintain convective self-aggregation at high SSTs.

To conclude, we show that the mechanisms involved in sustaining convective self-aggregation depend on the convective parameterization and that inaccuracies in the parameterization of convection may affect the degree of convective self-aggregation and thus the interaction with the large-scale circulation substantially. Different entrainment rates might explain to some degree why previous literature finds so many different paths to self-aggregation, in particular when convection is parameterized. Especially at high SSTs, a realistic convective parameterization is of crucial importance because convective self-aggregation is mostly constrained by thermodynamic processes that directly depend on the convective parameterization, that is, entrainment efficiency, static stability, and radiative cooling. From this perspective, it may well be that the most important task of a convective parameterization is to get the degree of convective aggregation right. An interesting approach might be to tune convective parameterizations based on some metric of convective aggregation in real-world simulations or observations.

This study emphasizes the importance of a realistic convective parameterization for modeling convective self-aggregation. Assumptions and uncertainties introduced by the convective parameterization have a strong influence on how the RCE climate organizes and responds to warming. With respect to climate change, this study implies that the entrainment rate is of particular importance for future projections because of its influence on large-scale convective self-aggregation at high SSTs.

**Acknowledgments**
The research was supported by the Max Planck Society for the Advancement of Science. Computing resources were provided by the German Climate Computing Center (DKRZ), Hamburg. Primary data and scripts used in the analysis and other supplementary information that may be useful in reproducing the author's work are archived by the Max Planck Institute for Meteorology and can be obtained by contacting publications@mpimet.mpg.de. The authors thank the internal reviewer Cheska Siongco and two external reviewers (Timothy Cronin and an anonymous reviewer) for their extremely thoughtful and helpful comments.

## References

Arakawa, A. (2004), The cumulus parameterization problem: Past, present, and future, *J. Clim.*, *17*(13), 2493–2525, doi:10.1175/1520-0442(2004)017 < 2493:RATCPP>2.0.CO;2.

Arakawa, A., and W. H. Schubert (1974), Interaction of a cumulus cloud ensemble with the large-scale environment, Part I, *J. Atmos. Sci.*, *31*(3), 674–701, doi:10.1175/1520-0469(1974)031 < 0674:IOACCE>2.0.CO;2.

Arnold, N. P., and D. A. Randall (2015), Global-scale convective aggregation: Implications for the MJO, *J. Adv. Model. Earth Syst.*, *7*, 1499–1518, doi:10.1002/2015MS000498.

Becker, T., and B. Stevens (2014), Climate and climate sensitivity to changing $CO_2$ on an idealized land planet, *J. Adv. Model. Earth Syst.*, *6*, 1205–1223, doi:10.1002/2014MS000369.

Beucler, T., and T. W. Cronin (2016), Moisture-radiative cooling instability, *J. Adv. Model. Earth Syst.*, *8*, 1620–1640, doi:10.1002/2016MS000763.

Bony, S., and K. A. Emanuel (2005), On the role of moist processes in tropical intraseasonal variability: Cloud–radiation and moisture–convection feedbacks, *J. Atmos. Sci.*, *62*(8), 2770–2789, doi:10.1175/JAS3506.1.

Bony, S., et al. (2015), Clouds, circulation and climate sensitivity, *Nat. Geosci.*, *8*(4), 261–268.

Bony, S., B. Stevens, D. Coppin, T. Becker, K. A. Reed, A. Voigt, and B. Medeiros (2016), Thermodynamic control of anvil cloud amount, *Proc. Natl. Acad. Sci. U. S. A.*, *113*(32), 8927–8932, doi:10.1073/pnas.1601472113.

Bretherton, C. S., and M. F. Khairoutdinov (2015), Convective self-aggregation feedbacks in near-global cloud-resolving simulations of an aquaplanet, *J. Adv. Model. Earth Syst.*, *7*, 1765–1787, doi:10.1002/2015MS000499.

Bretherton, C. S., and P. K. Smolarkiewicz (1989), Gravity waves, compensating subsidence and detrainment around cumulus clouds, *J. Atmos. Sci.*, *46*(6), 740–759, doi:10.1175/1520-0469(1989)046 < 0740:GWCSAD>2.0.CO;2.

Bretherton, C. S., P. N. Blossey, and M. F. Khairoutdinov (2005), An energy-balance analysis of deep convective self-aggregation above uniform SST, *J. Atmos. Sci.*, *62*(12), 4273–4292, doi:10.1175/JAS3614.1.

Cess, R. D., et al. (1989), Interpretation of cloud-climate feedback as produced by 14 atmospheric general circulation models, *Science*, *245*(4917), 513–516, doi:10.1126/science.245.4917.513.

Cess, R. D., et al. (1990), Intercomparison and interpretation of climate feedback processes in 19 atmospheric general circulation models, *J. Geophys. Res.*, *95*(D10), 16,601–16,615, doi:10.1029/JD095iD10p16601.

Cess, R. D., et al. (1996), Cloud feedback in atmospheric general circulation models: An update, *J. Geophys. Res.*, *101*(D8), 12,791–12,794, doi:10.1029/96JD00822.

Coppin, D., and S. Bony (2015), Physical mechanisms controlling the initiation of convective self-aggregation in a general circulation model, *J. Adv. Model. Earth Syst.*, *7*, 2060–2078, doi:10.1002/2015MS000571.

Craig, G. C., and J. M. Mack (2013), A coarsening model for self-organization of tropical convection, *J. Geophys. Res.*, *118*(16), 8761–8769, doi:10.1002/jgrd.50674.

Emanuel, K., A. A. Wing, and E. M. Vincent (2014), Radiative-convective instability, *J. Adv. Model. Earth Syst.*, *6*, 75–90, doi:10.1002/2013MS000270.

Fläschner, D., T. Mauritsen, and B. Stevens (2016), Understanding the inter-model spread in global-mean hydrological sensitivity, *J. Clim.*, *29*(2), 801–817, doi:10.1175/JCLI-D-15-0351.1.

Held, I. M., and B. J. Soden (2006), Robust responses of the hydrological cycle to global warming, *J. Clim.*, *19*, 5686–5699.

Held, I. M., R. S. Hemler, and V. Ramaswamy (1993), Radiative-convective equilibrium with explicit two-dimensional moist convection, *J. Atmos. Sci.*, *50*, 3909–3927, doi:10.1175/1520-0469(1993)050 < 3909:RCEWET>2.0.CO;2.

Hohenegger, C., and B. Stevens (2016), Coupled radiative convective equilibrium simulations with explicit and parameterized convection, *J. Adv. Model. Earth Syst.*, *8*, 1468–1482, doi:10.1002/2016MS000666.

Holloway, C. E., and S. J. Woolnough (2016), The sensitivity of convective aggregation to diabatic processes in idealized radiative-convective equilibrium simulations, *J. Adv. Model. Earth Syst.*, *8*, 166–195, doi:10.1002/2015MS000511.

Jeevanjee, N., and D. M. Romps (2013), Convective self-aggregation, cold pools, and domain size, *Geophys. Res. Lett.*, *40*, 994–998, doi:10.1002/grl.50204.

Khairoutdinov, M. F., and K. A. Emanuel (2010), Aggregated convection and the regulation of tropical climate, in *Extended Abstracts, 29th Conf. on Hurricanes and Tropical Meteorology*, Am. Meteorol. Soc., Tucson, Ariz.

Mapes, B. E. (2016), Gregarious convection and radiative feedbacks in idealized worlds, *J. Adv. Model. Earth Syst.*, *8*, 1029–1033, doi:10.1002/2016MS000651.

Möbis, B., and B. Stevens (2012), Factors controlling the position of the intertropical convergence zone on an aquaplanet, *J. Adv. Model. Earth Syst.*, *4*, M00A04, doi:10.1029/2012MS000199.

Muller, C. J., and S. Bony (2015), What favors convective aggregation and why?, *Geophys. Res. Lett.*, *42*, 5626–5634, doi:10.1002/2015GL064260.

Muller, C. J., and I. M. Held (2012), Detailed investigation of the self-aggregation of convection in cloud-resolving simulations, *J. Atmos. Sci.*, *69*(8), 2551–2565, doi:10.1175/JAS-D-11-0257.1.

Muller, C. J., P. A. O'Gorman, and L. E. Back (2011), Intensification of precipitation extremes with warming in a cloud-resolving model, *J. Clim.*, *24*(11), 2784–2800, doi:10.1175/2011JCLI3876.1.

Nesbitt, S. W., E. J. Zipser, and D. J. Cecil (2000), A census of precipitation features in the tropics using TRMM: Radar, ice scattering, and lightning observations, *J. Clim.*, *13*(23), 4087–4106.

Nordeng, T. E. (1994), *Extended Versions of the Convective Parametrization Scheme at ECMWF and Their Impact on the Mean and Transient Activity of the Model in the Tropics*, ECMWF Tech. Memo. 206, Eur. Cent. for Medium-Range Weather Forecasts, Reading, U. K.

O'Gorman, P. A., and C. J. Muller (2010), How closely do changes in surface and column water vapor follow Clausius-Clapeyron scaling in climate change simulations?, *Environ. Res. Lett.*, *5*(2), 025,207.

Oueslati, B., and G. Bellon (2013), Convective entrainment and large-scale organization of tropical precipitation: Sensitivity of the CNRM-CM5 hierarchy of models, *J. Clim.*, *26*(9), 2931–2946, doi:10.1175/JCLI-D-12-00314.1.

Pincus, R., and B. Stevens (2013), Paths to accuracy for radiation parameterizations in atmospheric models, *J. Adv. Model. Earth Syst.*, *5*, 225–233, doi:10.1002/jame.20027.

Popke, D., B. Stevens, and A. Voigt (2013), Climate and climate change in a radiative convective equilibrium version of ECHAM6, *J. Adv. Model. Earth Syst.*, *5*, 1–14, doi:10.1029/2012MS000191.

Ramanathan, V., and J. A. Coakley (1978), Climate modeling through radiative-convective models, *Rev. Geophys. Space Phys.*, *16*(4), 465–489.

Randall, D., M. Khairoutdinov, A. Arakawa, and W. Grabowski (2003), Breaking the cloud parameterization deadlock, *Bull. Am. Meteorol. Soc.*, *84*(11), 1547–1564, doi:10.1175/BAMS-84-11-1547.

Raymond, D. J. (1997), *Boundary Layer Quasi-Equilibrium (BLQ)*, pp. 387–397, Springer, Dordrecht, Netherlands, doi:10.1007/978-94-015-8828-7_15.

Reed, K. A., B. Medeiros, J. T. Bacmeister, and P. H. Lauritzen (2015), Global radiative-convective equilibrium in the community atmosphere model, version 5, *J. Atmos. Sci.*, *72*(5), 2183–2197, doi:10.1175/JAS-D-14-0268.1.

Singh, M. S., and P. A. O'Gorman (2013), Influence of entrainment on the thermal stratification in simulations of radiative-convective equilibrium, *Geophys. Res. Lett.*, *40*, 4398–4403, doi:10.1002/grl.50796.

Sobel, A. H., and C. S. Bretherton (2000), Modeling tropical precipitation in a single column, *J. Clim.*, *13*(24), 4378–4392.

Stein, T. H. M., C. E. Holloway, I. Tobin, and S. Bony (2017), Observed relationships between cloud vertical structure and convective aggregation over tropical ocean, *J. Clim.*, *30*(6), 2187–2207, doi:10.1175/JCLI-D-16-0125.1.

Stevens, B., and S. Bony (2013), What are climate models missing?, *Science*, *340*(6136), 1053–1054, doi:10.1126/science.1237554.

Stevens, B., S. Bony, and M. Webb (2012), *Clouds On-Off Klimate Intercomparison Experiment (COOKIE)*. [Available at http://www.euclipse.eu/wp4/wp4.html.]

Stevens, B., et al. (2013), Atmospheric component of the MPI-M Earth System Model: ECHAM6, *J. Adv. Model. Earth Syst.*, *5*, 146–172, doi:10.1002/jame.20015.

Tiedtke, M. (1989), A comprehensive mass flux scheme for cumulus parameterization in large-scale models, *Mon. Weather Rev.*, *117*(8), 1779–1800, doi:10.1175/1520-0493(1989)117 < 1779:ACMFSF>2.0.CO;2.

Tobin, I., S. Bony, and R. Roca (2012), Observational evidence for relationships between the degree of aggregation of deep convection, water vapor, surface fluxes, and radiation, *J. Clim.*, *25*, 6885–6904.

Tomassini, L., A. Voigt, and B. Stevens (2015), On the connection between tropical circulation, convective mixing, and climate sensitivity, *Q. J. R. Meteorol. Soc.*, *141*(689), 1404–1416, doi:10.1002/qj.2450.

Tompkins, A. M., and A. G. Semie (2017), Organization of tropical convection in low vertical wind shears: Role of updraft entrainment, *J. Adv. Model. Earth Syst.*, *9*, doi:10.1002/2016MS000802.

Webb, M. J., et al. (2015), The impact of parametrized convection on cloud feedback, *Philos. Trans. R. Soc. A*, *373*(2054), doi:10.1098/rsta.2014.0414.

Wing, A. A., and T. W. Cronin (2016), Self-aggregation of convection in long channel geometry, *Q. J. R. Meteorol. Soc.*, *142*(694), 1–15, doi:10.1002/qj.2628.

Wing, A. A., and K. A. Emanuel (2014), Physical mechanisms controlling self-aggregation of convection in idealized numerical modeling simulations, *J. Adv. Model. Earth Syst.*, *6*, 59–74, doi:10.1002/2013MS000269.